

Cite this article as: Xue Yuan, Shan Guibin, Pan Ruilin, et al. Research Progress of Al-Ti-V-based Lightweight High-Entropy Alloys[J]. Rare Metal Materials and Engineering, 2024, 53(01): 56-69. DOI: 10.12442/j.issn.1002-185X.E20230042.

REVIEW

Research Progress of Al-Ti-V-based Lightweight High-Entropy Alloys

Xue Yuan, Shan Guibin, Pan Ruilin, Tang Song, Lan Si

School of Materials Science and Engineering, Nanjing University of Science and Technology, Nanjing 210094, China

Abstract: In recent years, high-entropy alloys (HEAs) have become the research hotspot in the field of metal structural materials because of their novel design concepts and excellent physicochemical properties. With the continuous popularization of lightweight alloy design concepts, the conception of “entropy regulation” has been widely used to develop new lightweight alloys. Lightweight HEAs (LHEAs) are a new type of low density HEAs based on lightweight alloy designs. Their development and design mainly combine the empirical parameter criteria, phase diagram calculations, and first-principles calculations. Al-Ti-V-based LHEAs attract much attention among various LHEAs due to their excellent mechanical properties, good high temperature oxidation resistance, and fine corrosion resistance. This paper summarized the research progress of Al-Ti-V-based LHEAs from the perspective of composition design, preparation methods, microstructures, and physicochemical properties. Meanwhile, the problems and challenges for Al-Ti-V-based LHEAs were also prospected.

Key words: lightweight high-entropy alloys; alloy design; preparation methods; microstructure; physicochemical properties

Yeh et al^[1] firstly proposed the high-entropy alloys (HEAs) as a novel multi-principal element alloy in 2004. The composition of HEAs is significantly different from that of conventional alloys which typically consist of one or two primary elements. However, HEAs contain five or more principal elements with each content of 5at% – 35at% . Therefore, no clear distinction exists between the primary and secondary elements^[2]. This unique alloy design concept qualifies HEAs for high entropy effect, diffusion retardation effect, lattice distortion, and cocktail effect^[3-4]. Moreover, HEAs generally exhibit superior properties compared with traditional alloys, and thus present development potential and promising application prospects^[5-11].

In the early development stage, the refractory elements (Mo, Nb, Zr, Hf, Ta), transition metals (Ni, Mn, Fe, Co, Cr), or rare earth elements (Te, Dy) are the research hotspot as HEA composition. These series of HEAs exhibit higher density compared with the traditional alloys^[12]. Recently, the lightweight HEAs (LHEAs) attract much attention with the trend of lightweight material development^[13]. LHEAs

generally refer to HEAs with density below 7 g/cm³. Compared with traditional alloys, LHEAs normally have high specific strength^[5], high specific hardness^[6], high-temperature oxidation resistance^[8], good corrosion resistance^[9], high fracture toughness^[14], and fine wear resistance^[15]. As a result, LHEAs show great potential in engineering applications.

Researchers have conducted extensive theoretical and experimental studies on LHEAs in recent years, actively seeking empirical guidelines for phase structure prediction and composition design for LHEAs. These guidelines include thermodynamic parameters, such as mixing entropy (ΔS_{mix}), mixing enthalpy (ΔH_{mix}), atomic size difference (δ), and valence electron concentration (VEC) ^[16]. With the rapid development of computational simulation techniques, the calculation of phase diagrams (CALPHAD) and first-principles computational methods have been used to predict phase formation and phase transitions in LHEAs.

Due to their relatively low atomic mass, similar atomic radius, electronegativity, and excellent chemical stability, Al, Ti, and V are ideal elements for LHEA design^[15]. To further

Received date: October 06, 2023

Foundation item: National Key R&D Program of China (2021YFA1200203); National Natural Science Foundation of China (52101142, 52222104); China Postdoctoral Science Foundation (2021M701714); Natural Science Foundation of Jiangsu Province (BK20220959, BK20200019); Jiangsu Funding Program for Excellent Postdoctoral Talent (2022ZB253)

Corresponding author: Shan Guibin, Ph. D., School of Materials Science and Engineering, Nanjing University of Science and Technology, Nanjing 210094, P. R. China, E-mail: gbshan@njjust.edu.cn

Copyright © 2024, Northwest Institute for Nonferrous Metal Research. Published by Science Press. All rights reserved.

regulate and improve the physicochemical properties of Al-Ti-V-based LHEAs, researchers conduct numerous investigations and found that the Al-Ti-V system exhibits excellent properties, including high hardness and high strength^[11]. Based on the current research status, this paper reviewed the current research results on Al-Ti-V-based LHEAs, including alloy composition design, fabrication methods, microstructures, and physicochemical properties. The challenges and issues of Al-Ti-V-based LHEAs were proposed, and the prospects of future development were also provided.

1 Design of Al-Ti-V-based LHEAs

Research on HEAs has been conducted over a decade. However, due to the large number of alloying elements involved in HEAs and the complex interactions between multiple principal elements, basic theory cannot be established to explain the phase structure evolution of HEAs. For the composition design of LHEAs, empirical parameter criteria are the most widely used approach. Simultaneously, simulations for alloy design also attract much attention, including the first-principles calculations and CALPHAD to predict the phase formation and phase evolution in LHEAs. In composition design, the selection of alloying elements is of paramount importance. Based on the desired HEA performance, various high-performance LHEAs with leveraged cocktail effect can be prepared by selecting different lightweight elements^[17]. Al, Ti, and V are optimal elements for LHEA design and production due to their relatively small atomic mass, similar atomic radii, electronegativity, and excellent chemical stability^[15]. Refractory elements, such as Zr, Cr, and Nb, can act as stabilizers in the body-centered cubic (bcc) phase and exhibit good solubility with Al, Ti, and V elements, therefore improving the mechanical properties of LHEAs. The addition of Si, B, and C elements can effectively influence the ordered-to-disordered transition temperature of LHEAs, thereby enhancing the strength and reducing the density. Table 1 provides relevant physical properties of the elements in Al-Ti-V-based LHEAs^[18].

In the initial stage of LHEAs development, the primary design method is the empirical parameter method which is based on the thermodynamics and Hume-Rothery rules, and it includes the parameters, such as mixing entropy (ΔS_{mix}), mixing enthalpy (ΔH_{mix}), thermodynamic parameters (Q), VEC, and atomic size difference δ .

Feng et al^[19] proposed a theoretical density calculation formula for LHEAs:

$$\rho = \frac{\sum_{i=1}^n C_i A_i}{\sum_{i=1}^n C_i A_i / \rho_i} \quad (1)$$

where C_i , A_i , and ρ_i are the atomic percentage, atomic mass, and density of the i th constituent element, respectively.

Zhang et al^[16] summarized the relationships between the microstructure of reported HEAs and their atomic size difference δ , mixing enthalpy (ΔH_{mix}), and mixing entropy (ΔS_{mix}), as follows:

Table 1 Relevant physical properties of constituent elements in Al-Ti-V-based LHEAs^[18]

Element	Density/ g·cm ⁻³	Structure at 25 °C	Atom radius/pm	Melting temperature/K	VEC
Mg	1.74	hcp	160.13	923	2
Si	2.33	Cubic	115.3	1687	4
B	2.46	hcp	82	2348	3
C	2.7	hcp	77.3	3742	4
Al	2.7	fcc	143.17	933	3
Ti	4.5	hcp	146.15	1941	4
V	6.12	bcc	131.6	2183	5
Zr	6.51	hcp	160.25	2128	4
Cr	7.19	bcc	124.9	2180	6
Nb	8.58	bcc	142.9	2750	5
Cu	8.94	fcc	127.8	1358	11

Note: hcp-close packed hexagonal; fcc-face centered cubic

$$\delta = \sqrt{\sum_{i=1}^n c_i \left(1 - \frac{r_i}{\bar{r}}\right)^2} \quad (2)$$

$$\Delta H_{\text{mix}} = \sum_{i=1, i \neq j}^n \Omega_{ij} c_i c_j \quad (3)$$

$$\Delta S_{\text{mix}} = -R \sum_{i=1}^n c_i \ln c_i \quad (4)$$

where c_i is the atomic percentage of the i th element; r_i is the atomic radius of the i th element; \bar{r} is the average atomic radius; n is the total number of elements; $\Omega_{ij}=4\Delta H_{ij}^{\text{mix}}$; $\Delta H_{ij}^{\text{mix}}$ is the enthalpy of mixing between the i th and j th elements with equimolar composition in the liquid using the Miedema model; R is the gas constant.

Zhang et al^[16] developed a method to predict phase formation in HEAs based on atomic size difference (δ), mixing enthalpy (ΔH_{mix}), and mixing entropy (ΔS_{mix}). The $\Delta H_{\text{mix}}-\delta$ criterion is proposed for HEA design, which suggests that when $-15 \text{ kJ}\cdot\text{mol}^{-1} < \Delta H_{\text{mix}} \leq 5 \text{ kJ}\cdot\text{mol}^{-1}$, $12 \text{ J}\cdot\text{K}^{-1}\cdot\text{mol}^{-1} < \Delta S_{\text{mix}} \leq 17.5 \text{ J}\cdot\text{K}^{-1}\cdot\text{mol}^{-1}$, and $\delta < 6.5\%$, the single-phase solid solution is formed. The $\Delta H_{\text{mix}}-\delta$ criterion primarily considers the influence of ΔH_{mix} on the thermodynamic stability of solid solutions whereas ignoring the influence of ΔS_{mix} . To more accurately predict the phase formation in HEAs, the contribution of ΔS_{mix} should be considered. Yang et al^[20] introduced a new parameter Q and further modified the criterion into Eq.(5), as follows:

$$\begin{cases} Q = \frac{T_m \Delta S_{\text{mix}}}{|\Delta H_{\text{mix}}|} \\ T_m = \sum_{i=1}^n C_i (T_m)_i \end{cases} \quad (5)$$

where $(T_m)_i$ stands for the melting point of the i th element.

Guo et al^[21] established VEC criterion, which relates to the solid solution phase structure in HEAs. According to the results in Ref. [21], when $\text{VEC} < 6.87$, there is a tendency to form bcc solid solutions. When $6.87 < \text{VEC} < 8.0$, there is a tendency to form mixed bcc+fcc solid solutions. When $\text{VEC} \geq 8.0$, there is a tendency to form fcc solid solutions. Guo et al^[21] introduced the formula to calculate VEC value, as follows:

$$\text{VEC} = \sum_{i=1}^n c_i(\text{VEC})_i \quad (6)$$

where $(\text{VEC})_i$ is the valence electron concentration of the i th element.

The current approach for composition design of LHEAs primarily relies on the empirical parameter methods coupled with CALPHAD and first-principles calculations as supplementary tools. Indeed, empirical parameter methods can predict the alloy composition for solid solution formation. Meanwhile, CALPHAD and first-principles calculations can effectively predict the intermediate phases formed during the solidification process and further provide insights into the phase structures. These approaches jointly investigate the phase behavior and microstructure of LHEAs. Stepanov et al.^[22] designed AlNbTiV LHEA with $\delta=3.14\%$, $\Omega=1.38$, and $\text{VEC}=4.25$ using empirical parameter criteria. The results indicate that a single-phase bcc solid solution forms in AlNbTiV LHEA. Qiu et al.^[23] employed the first-principles computational methods to study the microstructure and thermodynamic properties of AlTiVCr LHEA by constructing two supercells, where one represents the disordered bcc structure and the other represents the ordered B2 structure. The simulation calculations reveal that the ordered B2 structure exhibits lower Gibbs free energy at low temperatures compared with the disordered bcc structure, thus indicating better thermal stability, as shown in Fig.1. It is also confirmed that the AlTiVCr alloy exhibits single-ordered B2 structure, which is consistent with the simulation results. It is found that the first-principles calculations can effectively predict the phase formation law of LHEAs.

Feng et al.^[24] used CALPHAD-based high-throughput computational method and efficiently screened out LHEAs with precipitation strengthening effect from thousands of potential composition designs in the Al-Cr-Fe-Mn-Ti system,

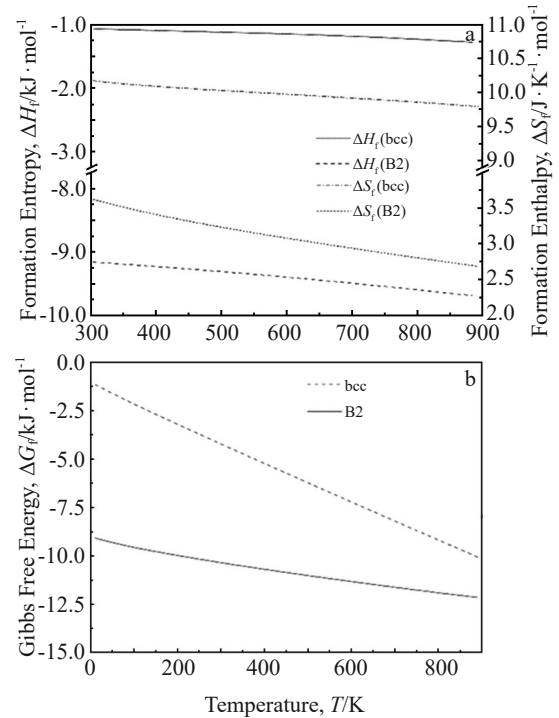


Fig.1 Formation entropy and formation enthalpy (a) as well as Gibbs formation energy (b) of bcc phase and B2 phase^[23]

as shown in Fig.2. It is confirmed that the alloys designed by CALPHAD-based high-throughput computational method exhibit higher strength at room temperature and at elevated temperatures. By summarizing and analyzing the strengthening mechanisms of ordered-to-disordered transformations, the accuracy of thermodynamic database for alloy prediction

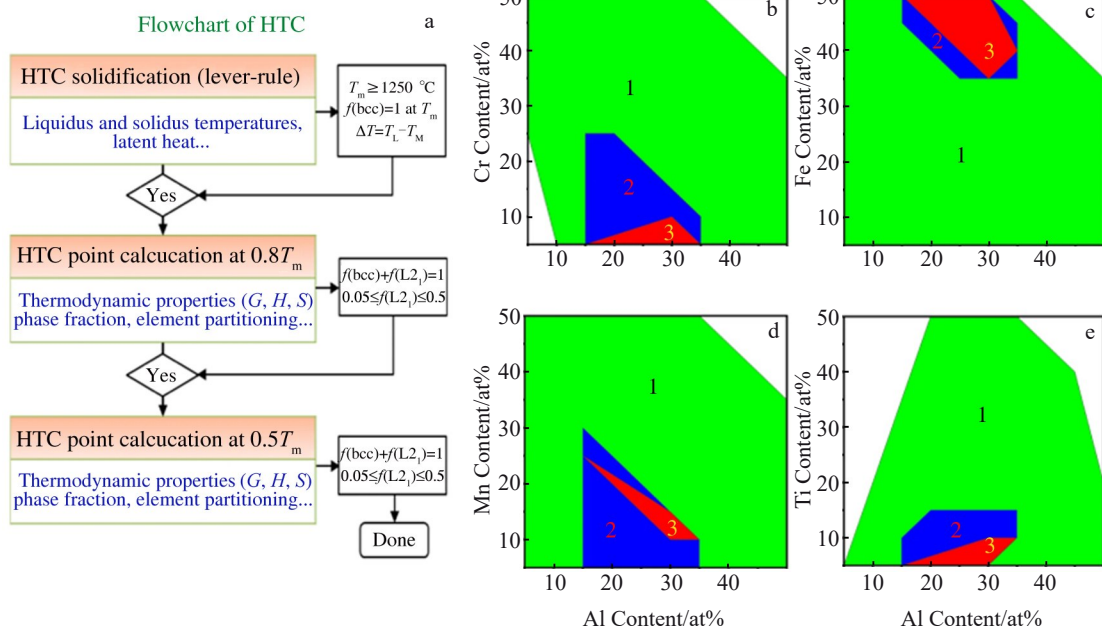


Fig.2 High-throughput screening flowchart (a) and results (b-e) of alloy composition in Al-Cr-Fe-Mn-Ti system^[24]

and design is further improved. It is demonstrated that combining high-throughput screening with multiscale modeling and experiment validation can effectively design the structural materials with outstanding performance.

Huang et al.^[25] used CALPHAD method to investigate the ordered-to-disordered phase transition in the AlCrTiV alloy system, as shown in Fig. 3. It is found that for the AlCrTiV alloy, increasing the Ti content can effectively lower the ordered-to-disordered transition temperature, subsequently reduce the degree of order in the alloy, and enhance the ductility. Based on the simulation results, the newly designed $\text{Al}_{10}\text{Cr}_{10}\text{Ti}_{70}\text{V}_{10}$ alloy exhibits excellent mechanical properties with appropriate tensile elongation (1.1%), yield strength (877 MPa), and ultimate tensile strength (889 MPa), demonstrating the promising potential for various applications.

2 Preparation Methods for Al-Ti-V-based LHEAs

2.1 Vacuum arc melting

The vacuum arc melting method involves the release of electric arc with tungsten electrodes under argon gas atmosphere to melt alloys, and the melting temperatures can reach above 3000 °C. LHEAs prepared by vacuum arc melting have the characteristics of fine and uniform grain structure and high density, which has several advantages, including rapid preparation, cost effectiveness, elevated melting temperature, and simple operation. Thus, the vacuum arc melting is the most widely employed technique to fabricate LHEAs. However, the prepared LHEAs usually exhibit compositional segregation and heightened internal stress, which seriously restricts the application of vacuum arc melting.

Yao et al.^[26] prepared $\text{Ti}_3\text{V}_2\text{NbAl}_{0.5}$ and $\text{Ti}_3\text{V}_2\text{NbAl}_{0.5}\text{Ni}_{0.5}$ alloys by arc melting, as shown in Fig. 4. It is revealed that $\text{Ti}_3\text{V}_2\text{NbAl}_{0.5}$ alloy exhibits single bcc structure, whereas the $\text{Ti}_3\text{V}_2\text{NbAl}_{0.5}\text{Ni}_{0.5}$ alloy consists of multi-phase structure: bcc phase+MgZn₂ (C14) structure+twinned B19' martensite. With the addition of Al and Ni elements, finer C14 Laves particles (approximately 0.2 μm) and twinned B19' martensite are precipitated on the dendritic grain boundaries of the $\text{Ti}_3\text{V}_2\text{NbAl}_{0.5}\text{Ni}_{0.5}$ alloy. The twinned B19' martensite is

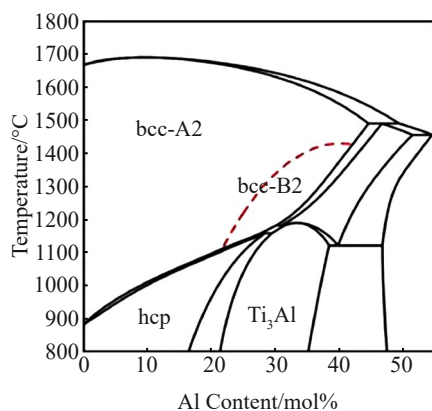


Fig.3 Phase diagram of Al-Ti binary alloy^[25]

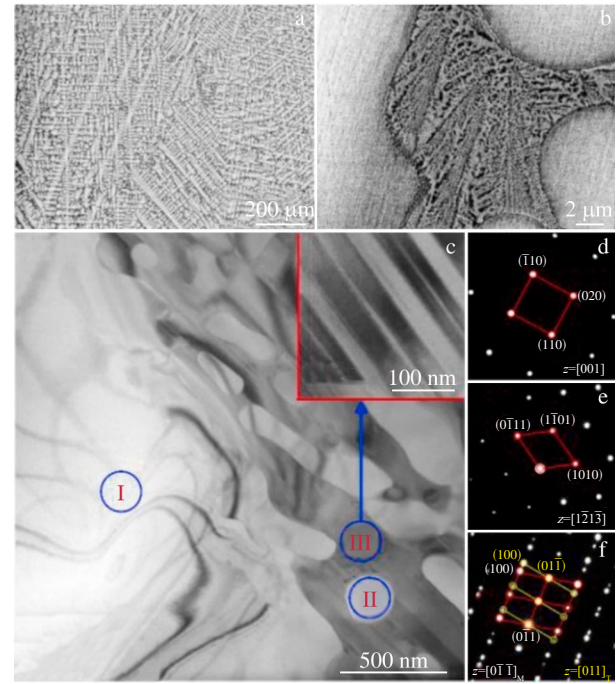


Fig.4 Microstructures of $\text{Ti}_3\text{V}_2\text{NbAl}_{0.5}\text{Ni}_{0.5}$ alloy at backscattered electron mode (a – b) and bright-field transmission electron mode (c); selected area electron diffraction patterns of region I (d), region II (e), and region III (f) in Fig.4c^[26]

surrounded by the C14 Laves phase and continuously distributed at the dendrite boundaries, reducing the secondary dendrite spacing. This phenomenon is favorable for solid solution strengthening, thereby increasing the yield strength of LHEAs. Furthermore, compared with the traditional dislocation deformation mechanisms, the formation of twins can provide new slip planes and thus improve the ductility of materials^[27]. Therefore, the $\text{Ti}_3\text{V}_2\text{NbAl}_{0.5}\text{Ni}_{0.5}$ alloy with low density (5.55 g/cm³) exhibits yield strength of 223 MPa and compressive ductility of 40% at room temperature, indicating better strength-ductility synergy, compared with other LHEAs.

2.2 Powder metallurgy

Different from vacuum arc melting, powder metallurgy involves the non-equilibrium solid-state alloying of powders at room temperature. The alloy powders are uniformly mixed through high-energy ball milling and then sintered into bulk materials with uniform composition. This method is suitable for LHEAs with significant differences in the melting points of alloying elements. Due to the constant collision, cold welding, and fracture of alloy powders during ball milling process, alloy atoms completely diffuse. By incorporating height heterogeneity and disorder of elements, the propensity for complex phase formation in alloys can be mitigated, thereby enhancing the thermal stability and mechanical properties. Consequently, the powder metallurgy-prepared alloys exhibit fine grain size, homogeneous composition, and exceptional performance^[28]. However, the potential introduction of impuri-

ties during the alloy ball milling process should be considered, and the long preparation duration and high manufacture cost restrict the wide application. Zhi et al^[29] manufactured the $\text{Al}_2\text{NbTi}_3\text{V}_2\text{Zr}_{0.4}$ alloy by high-energy ball milling and vacuum hot pressing. It is revealed that $\text{Al}_2\text{NbTi}_3\text{V}_2\text{Zr}_{0.4}$ alloy has yield strength of 1742 MPa, fracture strength of 2420 MPa, and compression strain of 38.2%, which are all better than those of other HEAs. Sun et al^[30] found that during the vacuum arc melting process of the alloys containing Mg or other alkali and alkaline earth metal elements, the intermetallic compounds easily form, leading to the decrease in alloy performance. However, the formation of complex phases is effectively suppressed during powder metallurgy due to the solute trapping effect. Additionally, the solid solution solubility is enhanced. As a result, the fine-grained alloys with exceptional properties can be obtained through powder metallurgy. Therefore, the powder metallurgy is an effective method to fabricate LHEAs containing alkali and alkaline earth metal elements.

2.3 Laser cladding

Laser cladding is a novel method to prepare LHEAs, which involves surface irradiation of substrate material by high-energy laser beam to simultaneously melt and solidify HEA cladding material. In this case, an alloy coating tightly attached to the substrate material is obtained^[31–32]. The alloy coatings prepared by laser cladding have exceptional substrate adhesion and uniform composition, which possess significant advantages in the enhancement of surface strength and corrosion resistance. However, the cost of laser cladding is high. Chen et al^[6] prepared a single-phase bcc AlTiVMoNb coating on the surface of Ti-6Al-4V (TC4) alloy by laser cladding. It is reported that the almost defect-free metallurgical bonding exists between AlTiVMoNb coating

and TC4 matrix, as shown in Fig. 5. Besides, the Vickers hardness of TC4 alloy after laser cladding increases from 3460.4 MPa to 8707.3 MPa.

3 Microstructure Characterization of Al-Ti-V-based LHEAs

Based on the microstructures of Al-Ti-V-based LHEAs, they can be divided into three types: single-phase microstructure, dual-phase microstructure, and multi-phase microstructure. Table 2 lists the density, phase composition, preparation method, and mechanical properties of Al-Ti-V-based LHEAs^[33].

3.1 Single-phase

The high entropy effect of HEAs increases the solubility between the primary elements and suppresses the formation of intermetallic compounds. Single-phase Al-Ti-V-based LHEAs typically exhibit the bcc or B2 structure. Stepanov et al^[22] prepared AlNbTiV LHEAs with density of approximately 5.59 g/cm^3 by arc melting method. It is found that both the as-cast and as-annealed alloys exhibit the single-phase bcc structure, as shown in Fig. 6. The as-cast alloy exhibits dendritic microstructure, whereas after homogenization annealing, the alloy exhibits equiaxed crystal organization with average grain size of $300\text{--}400 \mu\text{m}$. Liu et al^[40] designed AlNb_2TiV LHEA with low density of 6.19 g/cm^3 based on the empirical parameter criteria. This alloy consists of single B2 phase structure and exhibits high specific strength and excellent room-temperature plasticity.

3.2 Dual-phase

Although the high entropy effect of HEAs can suppress the formation of intermetallic compounds, the parameters ΔH_{mix} , δ , and VEC can also influence the phase structure of LHEAs. These parameters can promote the formation of precipitates

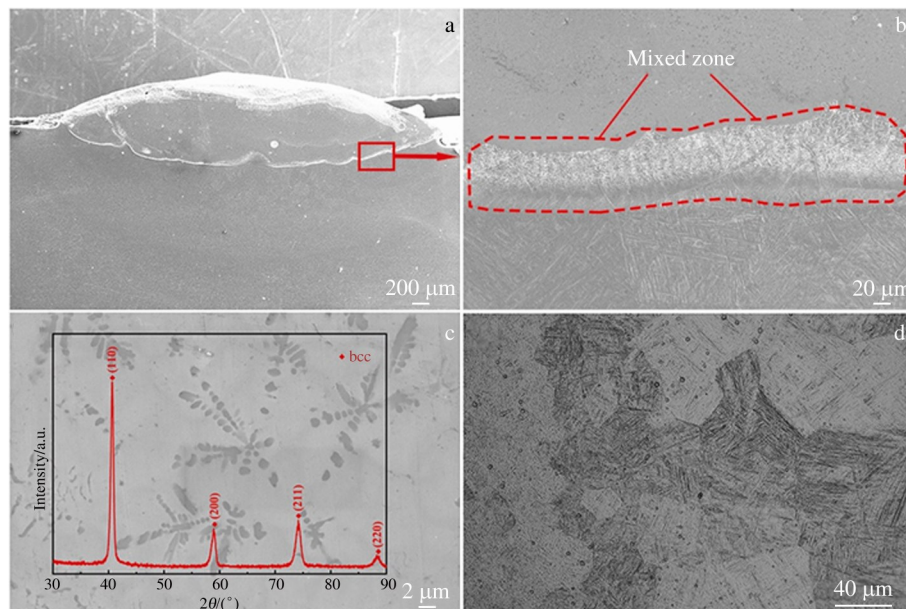


Fig.5 Microstructures of AlTiVNbMo coating and TC4 matrix: (a) cross-section morphology of coated sample; (b) mixing region; (c) cladding region; (d) heat-affected zone^[6]

Table 2 Preparation process, density, phase composition, and mechanical properties of Al-Ti-V-based LHEAs

Alloy	Preparation process	Density, ρ / $\text{g}\cdot\text{cm}^{-3}$	Phase composition	Yield stress/MPa	Fracture stress/ MPa	Fracture strain/%	Ref.
$\text{Ti}_{75}\text{Al}_{10}\text{V}_3\text{Cr}_5\text{Nb}_5$	AM	4.74	bcc	860	-	>50	[34]
$\text{Ti}_{60}\text{Al}_{18}(\text{VCrNb})_{22}$	AM	4.75	bcc	1269	-	>50	[5]
$\text{Ti}_{80}(\text{AlCrVNb})_{20}$	AM	4.79	bcc	600	-	>50	[7]
$\text{Ti}_{67}\text{Al}_{12}\text{V}_7\text{Cr}_7\text{Nb}_7$	AM	4.86	bcc	1065	-	>50	[34]
$\text{Ti}_{60}\text{Al}_{12}(\text{VCrNb})_{28}$	AM	5.03	bcc	960	1072	20	[5]
$\text{Ti}_{55}\text{Al}_{15}\text{V}_{10}\text{Cr}_{10}\text{Nb}_{10}$	AM	5.05	bcc	1465	1835	26	[34]
AlTiVCr	AM	5.06	B2	-	-	-	[23]
$\text{Ti}_{60}(\text{AlCrVNb})_{40}$	AM	5.09	bcc	821	-	>50	[7]
$\text{Ti}_{60}\text{Al}_{10}(\text{VCrNb})_{30}$	AM	5.12	bcc	938	1129	26	[5]
$\text{Ti}_{60}\text{Al}_8(\text{VCrNb})_{32}$	AM	5.21	bcc	920	1146	28.8	[5]
$\text{Ti}_{60}\text{Al}_6(\text{VCrNb})_{34}$	AM	5.31	bcc	895	1115	29	[5]
$\text{Ti}_3\text{V}_2\text{NbAl}_{0.5}$	AM	5.39	bcc	760	-	>50	[26]
$\text{Ti}_{40}(\text{AlCrVNb})_{60}$	AM	5.41	bcc	1122	1430	27	[7]
AlNbTiV	AM	5.59	bcc	1020	1318	5	[22]
AlCrNbTiV	AM	5.71	bcc	1550	1570	0.4	[35]
$\text{TiCrVNb}_{0.5}\text{Al}_{0.5}$	AM	5.76	bcc	-	-	-	[36]
$\text{Al}_{0.5}\text{CrNbTi}_2\text{V}_{0.5}$	AM	5.76	bcc	1240	-	>50	[37]
$\text{Ti}_{20}(\text{AlCrVNb})_{80}$	AM	5.81	bcc	-	-	-	[7]
$\text{Al}_{0.8}\text{NbTiVCo}_{0.2}$	AM	5.84	bcc	1473	-	>30	[38]
$\text{Al}_{0.8}\text{NbTiVNi}_{0.2}$	AM	5.84	bcc	1510	-	>30	[38]
$\text{Ti}_{30}\text{Al}_{20}\text{V}_{20}\text{Nb}_{20}\text{Mo}_{10}$	AM	5.88	bcc	1187	-	>50	[39]
$\text{Ti}_{35}\text{Al}_{15}\text{V}_{20}\text{Nb}_{20}\text{Mo}_{10}$	AM	6.03	bcc	971	-	>50	[39]
$\text{Ti}_{40}\text{Al}_{10}\text{V}_{20}\text{Nb}_{20}\text{Mo}_{10}$	AM	6.1	bcc	900	-	>50	[39]
AlNb ₂ TiV	AM	6.19	B2	1043	-	>30	[40]
AlCr _{0.5} NbTiV	AM	6.19	bcc	1300	1430	0.8	[35]
Al _{0.2} NbTiVZr	AM	6.29	bcc	1242	1585	11.94	[41]
Al _{0.1} NbTiVZr	AM	6.37	bcc	1177	1452	19.4	[41]
AlTiVMoNb	LC	6.43	bcc	-	-	-	[6]
$(\text{AlCrTiV})_{95}\text{Si}_5$	AM	4.74	B2+Ti ₅ Si ₃	-	-	-	[42]
$(\text{AlCrTiV})_{95}\text{C}_5$	AM	4.83	B2+TiC	-	-	-	[42]
$(\text{AlCrTiV})_{95}\text{B}_5$	AM	4.85	B2+TiB	-	-	-	[42]
$\text{Al}_2\text{NbTi}_3\text{V}_2\text{Zr}_{0.4}$	AM	5.05	bcc+Zr ₃ Al	1742	2420	38.2	[29]
$\text{TiZrV}_{0.5}\text{Nb}_{0.5}\text{Al}_{0.75}$	AM	5.44	bcc+Laves	-	-	-	[43]
AlNbTiVZr _{0.1}	AM	5.53	B2+Zr ₅ Al ₃	1290	1395	3.7	[44]
Al _{1.5} NbTiVZr	AM	5.55	B2+Laves	1310	1310	0	[45]
AlTiVCrCu _{0.4}	AM	5.55	bcc+hcp	1000	1000	5.5	[46]
$\text{Al}_{20}\text{Cr}_{10}\text{Nb}_{15}\text{Ti}_{20}\text{V}_{25}\text{Zr}_{10}$	AM	5.55	B2+Laves	1000	1000	0	[47]
AlNbTiVZr _{0.25}	AM	5.57	B2+Zr ₃ Al ₃	1360	1480	9.3	[44]
$\text{TiZrV}_{0.5}\text{Nb}_{0.5}\text{Al}_{0.5}$	AM	5.63	bcc+Laves	-	-	-	[43]
$\text{Al}_{0.5}\text{Nb}_{0.5}\text{TiV}_2\text{Zr}_{0.5}$	AM	5.76	bcc+Laves	1480	1771	14.1	[48]
AlCr _{1.5} NbTiV	AM	5.82	bcc+Laves	1700	-	-	[35]

Table 2 Preparation process, density, phase composition, and mechanical properties of Al-Ti-V-based LHEAs (continued)

Alloy	Preparation process	Density, ρ / $\text{g}\cdot\text{cm}^{-3}$	Phase composition	Yield stress/ MPa	Fracture stress/MPa	Fracture strain/%	Ref.
$\text{Al}_{0.5}\text{Nb}_{0.5}\text{TiV}_2\text{Zr}$	AM	5.85	bcc+Laves	1251	1262	7.3	[48]
$\text{TiZrV}_{0.5}\text{Nb}_{0.5}\text{Al}_{0.25}$	AM	5.85	bcc+Laves	-	-	-	[43]
$\text{Al}_{0.5}\text{NbTiV}_2\text{Zr}_{0.5}$	AM	6.06	bcc+Laves	1390	1723	16.9	[48]
$\text{Al}_{0.5}\text{NbTiVZr}$	AM	6.07	bcc+Laves	1264	1535	6.15	[41]
$\text{Al}_{0.5}\text{NbTiV}_2\text{Zr}$	AM	6.1	bcc+Laves	1028	1116	9.3	[48]
$\text{Al}_{0.4}\text{NbTiVZr}$	AM	6.14	bcc+Laves	1298	1590	9.29	[41]
$\text{Al}_{0.3}\text{NbTiVZr}$	AM	6.2	bcc+Laves	1367	1667	10.14	[41]
$\text{Al}_{17}\text{Ni}_{34}\text{Ti}_{17}\text{V}_{32}$	AM	6.21	bcc+L2 ₁	1527	3310	32	[49]
$\text{NbTiVZrAl}_{0.24}$	AM	6.34	bcc+Laves	1240	1730	5.4	[50]
$\text{Al}_{35}\text{Cr}_{14}\text{Mg}_6\text{Ti}_{35}\text{V}_{10}$	AM	4.05	bcc+FCC+HCP	1503	-	-	[51]
$\text{Al}_2\text{NbTi}_3\text{V}_2$	PM	4.93	bcc+AlV+Al ₂ Ti	2397	2674	15.7	[29]
$\text{Al}_{2.7}\text{TiVCrCu}$	AM	4.97	bcc+FCC+HCP	-	-	-	[52]
$\text{Al}_2\text{NbTi}_3\text{V}_2\text{Zr}_{0.2}$	PM	5.02	bcc+AlV+Al ₂ Ti	2322	2663	18.5	[29]
$\text{Al}_2\text{NbTi}_3\text{V}_2\text{Zr}_{0.6}$	PM	5.1	bcc+Zr ₃ Al+Ti ₂ ZrAl	2004	2581	28.1	[29]
$\text{Al}_2\text{NbTi}_3\text{V}_2\text{Zr}_{0.8}$	PM	5.18	bcc+Zr ₃ Al+Ti ₂ ZrAl	2098	2620	24.6	[29]
$\text{Al}_2\text{NbTi}_3\text{V}_2\text{Zr}$	PM	5.21	bcc+Zr ₃ Al+Ti ₂ ZrAl	2153	2625	19.8	[29]
$\text{Ti}_3\text{V}_2\text{NbNi}_{0.5}\text{Al}_{0.5}$	AM	5.55	bcc+Laves (C14)+B19'	1250	2750	40	[26]
AlCuTiVCr	LC	5.57	bcc ₁ +bcc ₂ +AlCuTi	-	-	-	[52]
$\text{AlNbTiVZr}_{0.5}$	AM	5.64	B2+Zr ₂ Al ₃ +Laves	1485	-	>50	[44]
$\text{AlNbTiVZr}_{0.5}$	AM	5.64	B2+Zr ₂ Al+Laves	1430	-	>50	[53]
AlNbTiVZr	AM	5.79	B2+Zr ₂ Al ₃ +Laves	1500	1675	3.0	[44]
AlNbTiVZr	AM	5.79	B2+Zr ₂ Al+Laves	1080	1210	2.3	[45]
$\text{AlNbTiVZr}_{1.5}$	AM	5.87	B2+Zr ₂ Al+Laves	1535	1550	0.4	[44]
$\text{Al}_{0.5}\text{Nb}_{0.5}\text{TiV}_2\text{Zr}_{1.5}$	AM	5.96	bcc+Laves (C14+C15)	797	835	5.1	[48]
$\text{TiAlV}_{0.5}\text{CrMo}$	PM	5.98	bcc ₁ +bcc ₂ +Al ₂ O ₃	1378	2085	8.5	[54]
$\text{Al}_{0.5}\text{NbTiV}_2\text{Zr}_{1.5}$	AM	6.17	bcc+Laves (C14+C15)	641	710	5.5	[48]
AlCrNbTiVZr	AM	6.25	bcc+Laves (ZrCrAl+ZrAl ₂)	1260	1270	0.2	[55]
$\text{Al}_{0.5}\text{CrNbTiVZr}$	AM	6.39	bcc+Laves (ZrCrAl+ZrAl ₂)	1630	1630	0	[55]
$\text{Al}_{0.25}\text{CrNbTiVZr}$	AM	6.5	bcc+Laves (ZrCrAl+ZrAl ₂)	1095	1095	0	[55]

Note: AM-arc melting; PM-powder metallurgy; LC-laser cladding

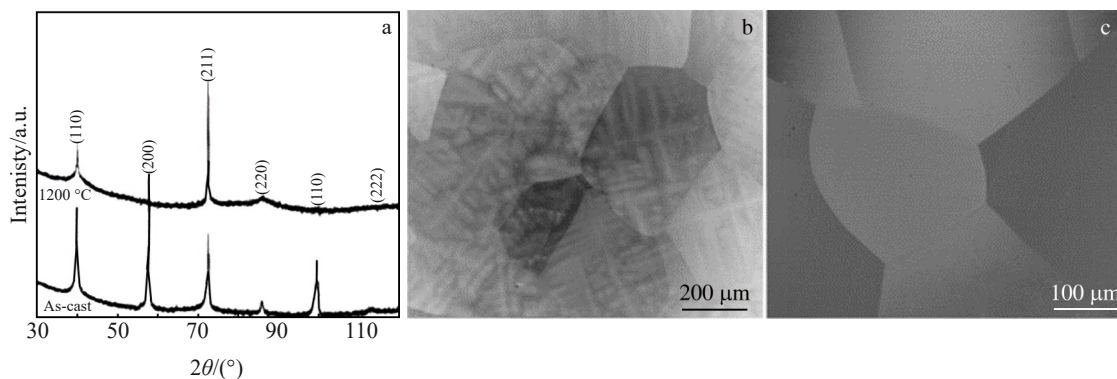


Fig.6 Phase structure analysis of AlNbTiV LHEA: (a) XRD pattern; (b-c) backscattered electron images^[40]

within the matrix. Xu et al^[41] investigated the influence of Al content ($x=0.1-0.5$) on the microstructure of $\text{Al}_x\text{NbTiVZr}$ HEAs, as shown in Fig. 7. When the aluminum content is

relatively low ($x=0.1, 0.2$), $\text{Al}_x\text{NbTiVZr}$ alloy exhibits the single-phase bcc microstructure. However, at higher aluminum contents ($x=0.3, 0.4, 0.5$), $\text{Al}_x\text{NbTiVZr}$ alloy

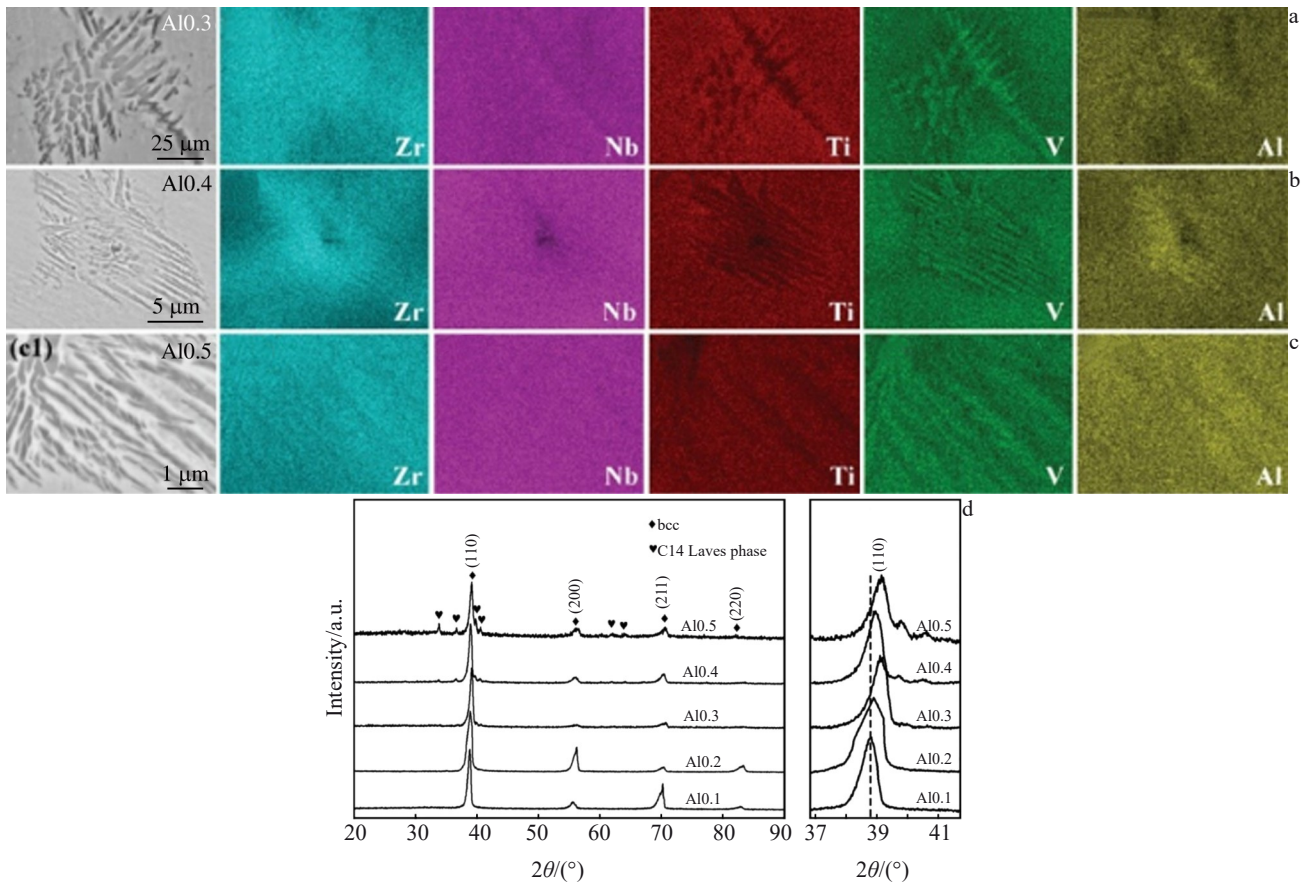


Fig.7 Element distribution maps of precipitated phase in as-cast Al_xNbTiVZr alloys: (a) $x=0.3$, (b) $x=0.4$, and (c) $x=0.5$; XRD patterns of as-cast Al_xNbTiVZr ($x=0.1-0.5$) alloys (d)^[41]

exhibits the dual-phase microstructure consisting of bcc and Laves phases. Additionally, according to the elemental distribution maps, it can be seen that with increasing the Al content, the morphology of Laves phase is changed significantly from coarse granular phase to fine lamellar structure. Jiang et al^[48] prepared Al_{0.5}NbTiV₂Zr_x and Al_{0.5}Nb_{0.5}TiV₂Zr_x LHEAs by vacuum arc melting and investigated the influence of Zr content on the microstructure and mechanical properties of these alloys. It is found that the alloys consist of dual-phase structure of bcc matrix phase+Laves phase, as shown in Fig. 8. With increasing the Zr content from $x=0.5$ to $x=1.5$, the volume fraction of bcc matrix phase is decreased, whereas that of Laves phase is increased. The Laves phase has high hardness, high melting point, but inferior plasticity. Therefore, with increasing the Zr content, the ductility of this alloy system is gradually decreased. Wang et al^[49] designed the lightweight, ultra-high strength, and highly thermally stable LHEA by incorporating an exceptionally stable Heusler (L₂₁) ordered phase and constructing a low lattice mismatch eutectic phase interface. Through arc melting based on the phase diagram simulations, the prepared Al₁₇Ni₃₄Ti₁₇V₃₂ alloy consists of L₂₁ and bcc phases. It is revealed that this alloy has remarkable yield strength (1527 MPa) and strain rate (>30%). Fig.9 shows the microstructure of as-cast alloy, and the dislocation networks

can be observed at the eutectic phase interfaces. The lattice mismatch between the eutectic bcc phase and L₂₁ phase is compensated by the pre-existing dislocations at phase interfaces. The interactions between the internal dislocations within phases and the interface dislocation networks significantly reduce the overall dislocation migration rate. This design strategy provides an effective approach for LHEA development.

3.3 Multi-phase

The lattice distortion and diffusion retardation effect in HEAs can hinder the nucleation and grain growth, thus forming complex multi-phase structures in LHEAs. These structures typically consist of solid solution phases (fcc, bcc, and hcp structures) and intermetallic compounds (Laves phase, σ phase, carbides, oxides). Zhi et al^[29] prepared multi-phase Al₂NbTi₃V₂Zr_x ($x=1.0, 0.8, 0.6, 0.4, 0.2, 0$) alloys by powder metallurgy. It is found that the types and quantities of precipitated phases in the Al₂NbTi₃V₂Zr_x system are influenced by the mixing enthalpy among the five elements. As shown in Fig.10, when the Zr content is relatively high, due to the low mixing enthalpy between Al and Zr/Ti, it is easy to form Zr₃Al-rich phases and Ti₂ZrAl-rich phases. The alloy microstructure consists of bcc solid solution matrix and two kinds of intermetallic compounds, namely Zr₃Al and Ti₂ZrAl.

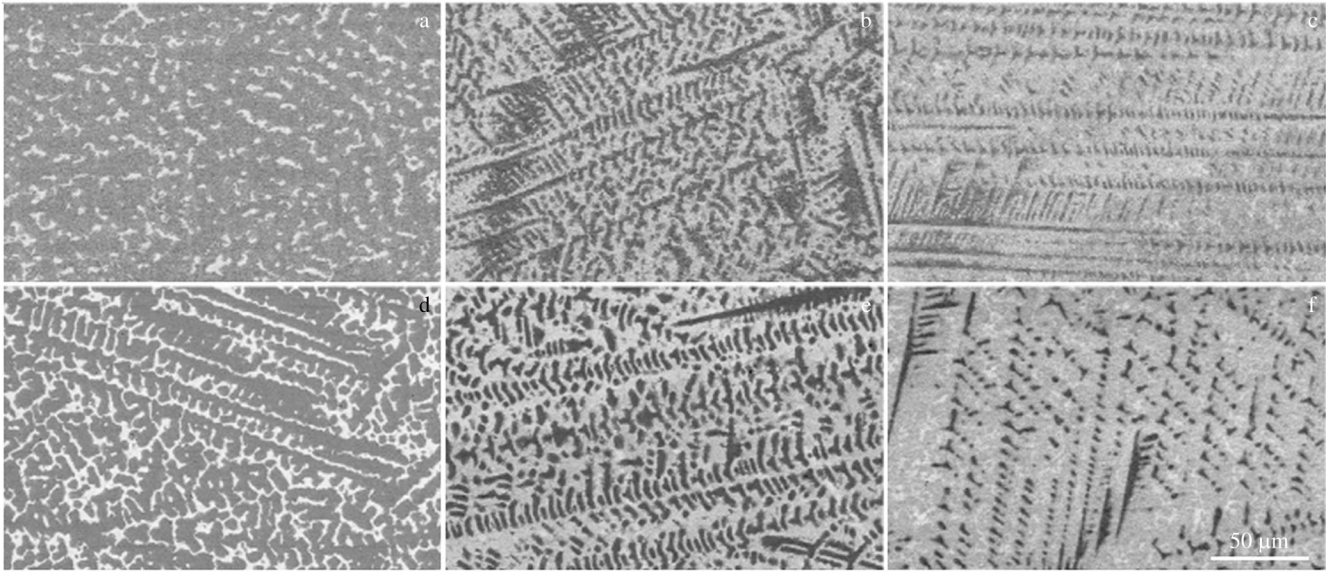


Fig.8 Backscattered electron images of $\text{Al}_{0.5}\text{NbTiV}_2\text{Zr}_x$ alloys with $x=0.5$ (a), $x=1.0$ (b), and $x=1.5$ (c); backscattered electron images of $\text{Al}_{0.5}\text{Nb}_{0.5}\text{TiV}_2\text{Zr}_x$ alloys with $x=0.5$ (d), $x=1.0$ (e), and $x=1.5$ (f)^[48]

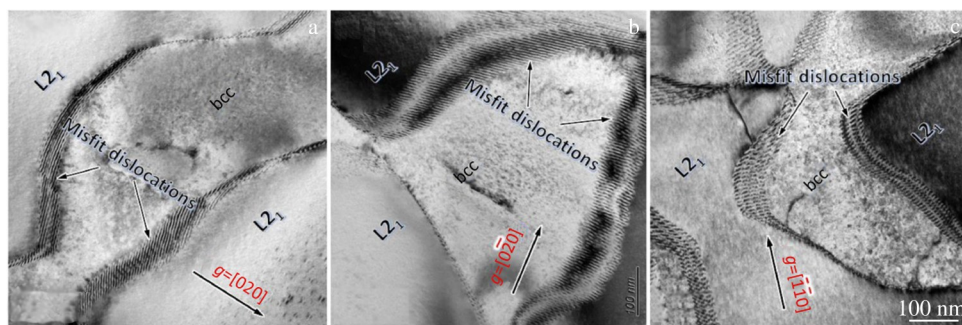


Fig.9 Microstructures of $\text{Al}_{17}\text{Ni}_{34}\text{Ti}_{17}\text{V}_{32}$ alloy along different orientations^[49]

When the Zr content decreases to $x=0.4$, the mixing enthalpy between Zr and Al (-44 mol/kJ) is lower than that between Ti and Al (-30 mol/kJ), and the mixing enthalpy of Zr_3Al phase (-39 mol/kJ) is lower than that of Ti_2ZrAl phase (-26 mol/kJ). As a result, the Zr_3Al phase is more stable compared with the Ti_2ZrAl phase, and the dissolution rate of Ti_2ZrAl phase is significantly faster than that of Zr_3Al phase. With further decreasing the Zr content, due to the high entropy effect, Zr element is more easily dissolved into the matrix to form solid solution. Consequently, the Zr_3Al phase gradually dissolves completely, and therefore new intermetallic compounds, such as Al_2Ti and AlV , are precipitated.

Gao et al^[54] prepared $\text{TiAlV}_{0.5}\text{CrMo}$ LHEAs with ultrafine grains by powder metallurgy. After ball milling, it is observed that the alloy powder consists of single-phase bcc oversaturated solid solution with nanocrystalline structure. During the ball milling process, the repeated cold welding and fracture between particles result in the single oversaturated bcc solid solution phase in the alloy powder. The phase transformation process is shown in Fig. 11. After plasma sintering, the alloy exhibits the multi-phase structure,

including the bcc phases enriched with V, Cr, and Mo, bcc phases enriched with Ti and V, and Al_2O_3 particles. High-density grain boundaries can store a significant amount of deformation energy, thus reducing the activation energy required for phase transformation, which facilitates the precipitation of bcc phases during plasma sintering. Additionally, the pulse current provides an extra driving force for atomic diffusion through electron-ion collisions during plasma sintering, promoting the nucleation of the secondary phase. Due to the inevitable oxygen contamination during ball milling and pulsed current plasma sintering and the oxygen affinity of Al element, Al_2O_3 particles can be absolutely observed in the sample.

4 Properties of Al-Ti-V-based LHEAs

The diverse phase structures and microstructural features of Al-Ti-V-based LHEAs can promote the physicochemical properties, but the research status is still in infancy. Currently, the researches mainly focus on the mechanical properties of LHEAs, whereas the high-temperature oxidation resistance and corrosion resistance are rarely investigated.

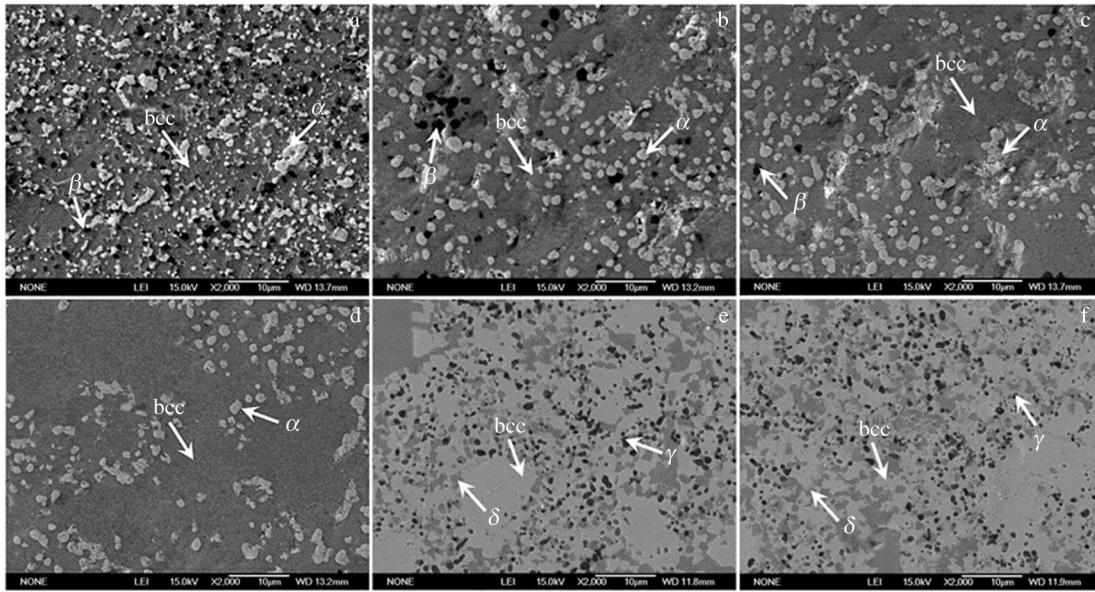


Fig.10 Microstructures of $Al_2NbTi_3V_2Zr_x$ alloys with $x=1.0$ (a), $x=0.8$ (b), $x=0.6$ (c), $x=0.4$ (d), $x=0.2$ (e), and $x=0$ (f)^[29]

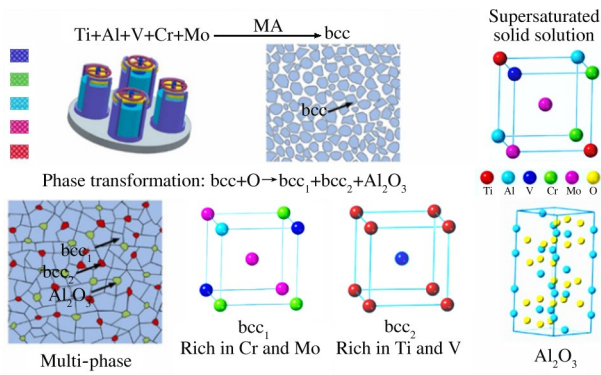


Fig.11 Schematic diagram of phase evolution during plasma sintering^[54]

4.1 Mechanical properties

Changes in element content, manufacturing process, and heat treatment process can all influence the mechanical properties of LHEAs. Zhang et al^[7] investigated the influence of Ti content on the mechanical properties of $Ti_x(AlCrVNb)_{100-x}$ ($x=20, 40, 60, 80$) alloys. Fig.12 shows the compressive stress-compressive strain curves of $Ti_x(AlCrVNb)_{100-x}$ alloys at room temperature. The yield strength of $Ti_{40}(AlCrVNb)_{60}$ alloy is 1122 MPa, and its ductility is 27%. In contrast, the $Ti_{60}(AlCrVNb)_{40}$ and $Ti_{80}(AlCrVNb)_{20}$ alloys exhibit low yield strength of 821 and 600 MPa, respectively. However, their ductility exceeds 50%. The microstructure characterizations are shown in Fig.13. It is revealed that the Ti content significantly influences the mechanical properties of $Ti_x(AlCrVNb)_{100-x}$ alloys. In the $Ti_{20}(AlCrVNb)_{80}$ alloy, brittleness is attributed to the phase separation at grain boundaries. With increasing the Ti content, the brittle phase gradually dissolves, significantly improving the alloy ductility.

Huang et al^[42] added B, C, and Si elements into AlCrTiV

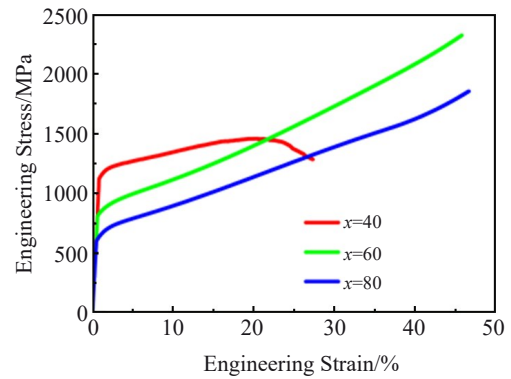


Fig.12 Compressive engineering stress-engineering strain curves of $Ti_x(AlCrVNb)_{100-x}$ alloys^[7]

alloy through microalloying and arc melting treatments to prepare $(AlCrTiV)_{100-x}C_x$, $(AlCrTiV)_{100-x}Si_x$, and $(AlCrTiV)_{100-x}B_x$ alloys. It is found that AlCrTiV alloy exhibits the single-phase bcc crystal structure. When B, C, and Si are added into AlCrTiV alloy, TiB, TiC, and Ti_5Si_3 are formed in the matrix, respectively. The incorporation of lightweight elements not only effectively reduces the density but also introduces precipitate phases, thereby enhancing the hardness of LHEAs. When 5at% B element is added into AlCrTiV alloy, the alloy exhibits high hardness of 6.96 GPa. This research provides a new perspective for LHEA design: adding a trace amount of non-metallic elements can significantly improve the mechanical properties of LHEAs, reduce the overall density, and decrease the preparation cost.

Chen et al^[6] deposited AlTiVMoNb LHEA coating on TC4 alloy substrate by laser cladding method. The coating exhibits the bcc single-phase structure with Vickers hardness of 8677.9 MPa, which is 152% higher than that of TC4 matrix. Compared with that of AlTiVMoNb alloy prepared by arc

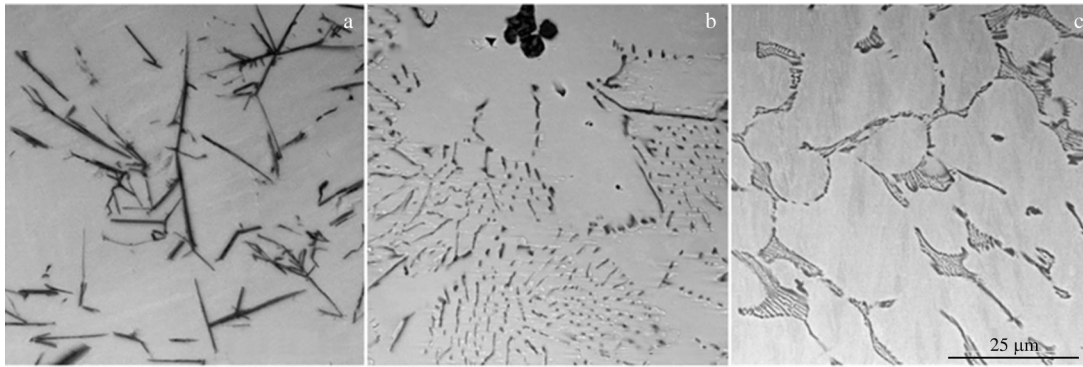


Fig.13 Microstructures of micro-alloyed AlCrTiV alloys: (a) $(\text{AlCrTiV})_{100-x}\text{B}_x$; (b) $(\text{AlCrTiV})_{100-x}\text{C}_x$; (c) $(\text{AlCrTiV})_{100-x}\text{Si}_x$ ^[42]

melting, the hardness increases by 66%. This result indicates that the mechanical properties of Al-Ti-V-based LHEAs depend on the specific manufacturing process. Stepanov et al^[34] investigated the influence of annealing on the mechanical properties of $\text{Al}_{0.5}\text{CrNbTi}_2\text{V}_{0.5}$ alloy. It is revealed that after annealing, due to the precipitation of Laves phases, the compressive yield strength of the alloy increases from 1240 MPa to 1340 MPa, demonstrating that different heat treatment processes can also significantly affect the mechanical properties of LHEAs.

4.2 High-temperature oxidation resistance

The formation of continuous, dense, and stable protective oxide film is crucial to the high-temperature oxidation resistance of Al-Ti-V-based LHEAs. Chen et al^[6] conducted high-temperature oxidation tests on the AlTiVMoNb-coated TC4 alloy, and the oxidation mass gain is shown in Fig. 14. The results reveal that the average oxidation mass gain of the AlTiVMoNb coating is only 10.58% of that of TC4 substrate (equivalent to 46.7 mg/cm²), indicating a significant improvement in the oxidation resistance of coated TC4 alloy at high temperatures. The high-temperature oxidation products of the AlTiVMoNb coating consist of complex oxides, including $\text{Al}_{0.2}\text{Nb}_{0.2}\text{Ti}_{0.6}\text{O}_2$, AlMoVO_7 , and $\text{Nb}_{10.7}\text{V}_{2.38}\text{O}_{32.7}$. The presence of this composite layer effectively reduces the diffusion pathways for oxygen atoms, thereby significantly enhancing the oxidation resistance of LHEAs.

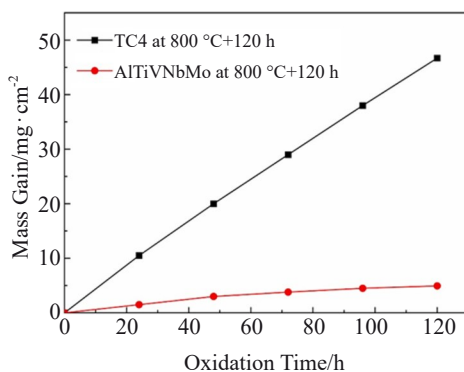


Fig.14 Oxidation mass gain of TC4 alloy and AlTiVMoNb coating at 800 °C^[6]

Esmaily et al^[8] investigated the high-temperature oxidation resistance of AlTiVCr LHEA. Fig.15 shows the microstructure and element distribution maps of AlTiVCr alloy after oxidation at 900 °C for 24 h. According to the microstructure characterization, after high-temperature oxidation, the uppermost layer of the alloy consists of V_2O_5 , the intermediate layer contains TiO_2 with Cr, V, and $(\text{Al, Cr})_2\text{O}_3$, and the inner layer is composed of TiO_2 and Al_2O_3 . The AlTiVCr alloy forms a multilayered oxide film during the high-temperature oxidation, effectively reducing the oxidation rate and thereby enhancing the oxidation resistance of LHEAs.

4.3 Corrosion resistance

The unique cocktail effect of HEAs ensures the excellent corrosion resistance of Al-Ti-V-based LHEAs^[28]. Tan et al^[56] investigated the corrosion resistance of $\text{Al}_2\text{NbTi}_3\text{V}_2\text{Zr}$ alloy in 10wt% HNO_3 solution. Fig.16 shows the polarization curves of $\text{Al}_2\text{NbTi}_3\text{V}_2\text{Zr}$ alloys prepared at different sintering temperatures during immersion in 10wt% HNO_3 solution. The experiment results show that the self corrosion current density of the $\text{Al}_2\text{NbTi}_3\text{V}_2\text{Zr}$ alloy varies from $1.90 \times 10^{-6} \text{ A} \cdot \text{cm}^{-2}$ to $4.47 \times 10^{-6} \text{ A} \cdot \text{cm}^{-2}$, which is lower by 1–2 orders of magnitude than that of titanium alloys ($4.09 \times 10^{-4} \text{ A} \cdot \text{cm}^{-2}$). This result indicates that the corrosion resistance of the $\text{Al}_2\text{NbTi}_3\text{V}_2\text{Zr}$ alloy is significantly better than that of titanium alloys. The microstructure of $\text{Al}_2\text{NbTi}_3\text{V}_2\text{Zr}$ alloy consists of bcc phase and Zr_3Al phase. The uneven distribution of elements within the Zr_3Al phase leads to significant local difference in free energy, leading to easy corrosion during the polarization process. With increasing the sintering temperature, the corrosion resistance of alloys is gradually improved due to the gradual reduction of Zr_3Al phase in the alloy. The $\text{Al}_2\text{NbTi}_3\text{V}_2\text{Zr}$ alloy prepared by sintering at 1350 °C exhibits excellent corrosion resistance. However, with further increasing the sintering temperature, the grain boundaries are coarsened, reducing the density of passivation film and gradually degrading the corrosion resistance of materials.

Additionally, the investigations of corrosion resistance of Al-Ti-V-based LHEAs in NaCl solution are widely conducted. Qiu et al^[9] studied the corrosion behavior of AlTiVCr alloy in 0.6 mol/L NaCl solution. Fig.17 provides the potentiodynamic polarization curves of as-cast AlTiVCr alloy in 0.6 mol/L

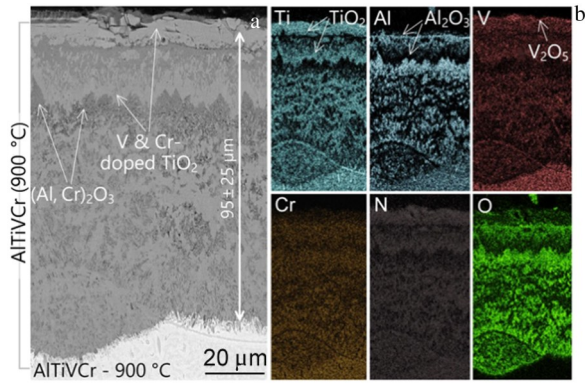


Fig.15 Microstructures (a) and elemental distribution maps (b) of AlTiVCr LHEA after oxidation at 900 °C^[8]

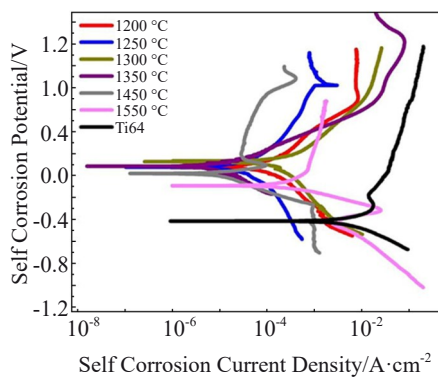


Fig.16 Potentiodynamic polarization curves of Al₂NbTi₃V₂Zr alloy and TC4 alloy at different temperatures^[56]

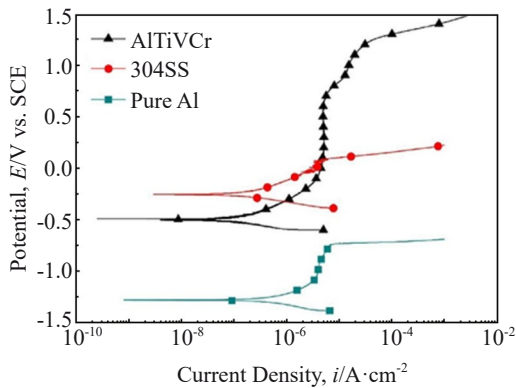


Fig.17 Potentiodynamic polarization curves of as-cast AlTiVCr alloy, 304 stainless steels, and pure Al in 0.6 mol/L NaCl at 25 °C^[9]

NaCl at 25 °C. After polarization in 0.6 mol/L NaCl solution, a dense multilayer passivation film containing Al₂O₃, TiO₂, Cr₂O₃, and V₂O₃ forms on the AlTiVCr alloy surface. Compared with the single-layer passive films formed on the surfaces of pure Al and 304 stainless steel, this dense multilayer passive film can better prevent the initiation of pitting corrosion. The presence of Cr₂O₃ and V₂O₃ in the passive film undergoes passivation dissolution during anodic

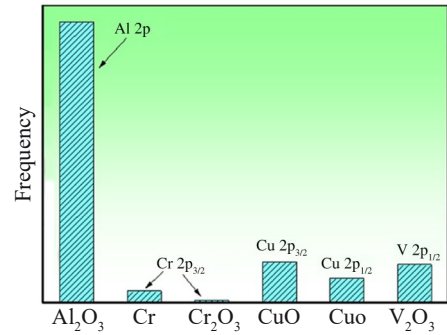


Fig.18 Composition of passivation film on AlTiVCrCu_{0.4} HEA surface^[46]

polarization, increasing the electrolyte acidity, which in turn slightly promotes the overpassivation dissolution of Al₂O₃ within the passive film. However, the AlTiVCr alloy also exhibits significantly high pit corrosion potential of $E_{pit} = 1274$ mV vs. SCE with much wider passive window (1745 mV vs. SCE) during anodic polarization, indicating excellent corrosion resistance.

Liu et al^[46] prepared the AlTiVCrCu_{0.4} alloy with dual-phase structure (86% bcc and 14% hcp) by arc melting and discussed its corrosion resistance in 0.6 mol/L NaCl solution. Fig. 18 shows the composition proportion of the passivation film on the surface of AlTiVCrCu_{0.4} alloy. It is found that the main components of the passivation film are oxides of Al, Cu, and V elements, and unoxidized Cr atoms also exist. Compared with the traditional single-layer oxide-based protective film, this composite protective film composed of metal oxides and unoxidized metal atoms has better corrosion resistance. The corrosion current density of the modified AlTiVCrCu_{0.4} alloy is 1.369×10^{-7} A/cm², and the corrosion potential is -0.534 V vs. SCE, which is lower than that of 304 stainless steel (-0.272 V vs. SCE), demonstrating excellent corrosion resistance.

5 Conclusions and Outlook

Al-Ti-V-based light high-entropy alloys (LHEAs) not only exhibit outstanding properties of traditional high-entropy alloys, such as high strength, high hardness, good corrosion resistance, and fine high-temperature oxidation resistance, but also show exceptional specific strength and specific hardness due to their low-density characteristics, presenting promising applications in aerospace and high-tech fields. However, the development of high-performance Al-Ti-V-based LHEAs is still in the initial stage. In recent years, the researches mainly focus on the preparation methods and mechanical properties, especially the hardness and compression properties. The fatigue resistance, high-temperature creep resistance, radiation resistance, and frictional wear resistance are also crucial for engineering applications, but these properties are rarely investigated. There may be three main reasons for the aforementioned problems. Firstly, the design theory of Al-Ti-V-based LHEAs is incomplete, which is a big challenge for

efficient design of high-performance LHEAs. Secondly, due to the processing limitation, the production of LHEAs heavily relies on the vacuum melting methods, which restricts the property enhancement and practical applications. Thirdly, the current alloy system has inferior ductility and almost no plasticity, which further restricts the practical applications. Therefore, to design and prepare Al-Ti-V-based LHEAs, it is crucial to address the following points:

1) Develop a comprehensive design theory for Al-Ti-V-based LHEAs. Currently, there is insufficient data support and theoretical basis for the design of Al-Ti-V-based LHEAs. The commonly used empirical parameter methods, phase diagram calculations, and first-principles calculations for alloy design cannot perfectly predict and control the phase composition and phase transformations of alloys. Therefore, developing and establishing a database for Al-Ti-V-based LHEAs can effectively predict the phase structure of alloys, thereby forming the relationship between structure and property and promoting the design of high-performance Al-Ti-V-based LHEAs.

2) Ameliorate the preparation processes for Al-Ti-V-based LHEAs. Fabrication of Al-Ti-V-based LHEAs primarily relies on the traditional arc melting methods, resulting in complex phase structures and therefore difficulty control of alloy properties. Although the new fabrication methods, such as powder metallurgy and additive manufacturing, can produce single-phase high-performance Al-Ti-V-based LHEAs, their efficiency is relatively low and the production cost is high. The thermal stability of Al-Ti-V-based LHEAs should be further improved.

3) Modify the mechanical properties of Al-Ti-V-based LHEAs. Currently, the Al-Ti-V-based LHEAs predominantly consist of body-centered cubic (bcc) phase and intermetallic compounds. Due to the limited slip systems for deformation in the bcc structure, dislocation slip is relatively challenging, leading to lower plasticity of Al-Ti-V-based LHEAs. The microstructures of Al-Ti-V-based LHEAs should be further researched by introducing face-centered cubic phase structure with strong deformation ability into the matrix, thus creating multi-phase heterogeneous structures to enhance the plasticity. Additionally, the methods, such as transformation-induced plasticity and twin-induced plasticity, can be attempted to improve the ductility of LHEAs.

References

- 1 Yeh J W, Chen S K, Lin S J et al. *Advanced Engineering Materials*[J], 2004, 6(5): 299
- 2 Zhang Y. *High-Entropy Materials*[M]. Berlin: Springer, 2019
- 3 Li R X, Geng G, Zhang Y. *MRS Communications*[J], 2023, 13: 740
- 4 Lu Yidi, Zhang Xiaoyong, Hou Shuo et al. *Rare Metal Materials and Engineering*[J], 2021, 50(1): 333 (in Chinese)
- 5 Liao Y C, Ye W T, Chen P S et al. *Intermetallics*[J], 2021, 135: 107213
- 6 Chen L, Wang Y, Hao X et al. *Vacuum*[J], 2021, 183: 109823
- 7 Zhang X K, Huang J C, Lin P H et al. *Journal of Alloys and Compounds*[J], 2020, 831: 184752
- 8 Esmaily M, Qiu Y, Bigdeli S et al. *NPJ Materials Degradation*[J], 2020, 4(1): 25
- 9 Qiu Y, Thomas S, Gibson M A et al. *Corrosion Science*[J], 2018, 133: 386
- 10 Wang J J, Zhao N, Yan M Y et al. *Scripta Materialia*[J], 2023, 229: 115374
- 11 Liu X M, Kou Z D, Qu R T et al. *Journal of Materials Science & Technology*[J], 2023, 143: 62
- 12 George E P, Raabe D, Ritchie R O. *Nature Reviews Materials*[J], 2019, 4(8): 515
- 13 Zhao Haichao, Qiao Yulin, Liang Xiubing et al. *Rare Metal Materials and Engineering*[J], 2020, 49(4): 1457 (in Chinese)
- 14 Yurchenko N Y, Stepanov N D, Gridneva A O et al. *Journal of Alloys and Compounds*[J], 2018, 757: 403
- 15 Jeong I S, Lee J H. *Materials & Design*[J], 2023, 227: 111709
- 16 Zhang Y, Zhou Y J, Lin J P et al. *Advanced Engineering Materials*[J], 2008, 10(6): 534
- 17 Lin G X, Guo R P, Shi X H et al. *Entropy*[J], 2022, 24(12): 1777
- 18 Miracle D B, Senkov O N. *Acta Materialia*[J], 2017, 122: 448
- 19 Feng R, Gao M, Lee C et al. *Entropy*[J], 2016, 18(9): 333
- 20 Yang X, Zhang Y. *Materials Chemistry and Physics*[J], 2012, 132(2-3): 233
- 21 Guo S, Ng C, Lu J et al. *Journal of Applied Physics*[J], 2011, 109(10): 103505
- 22 Stepanov N D, Shaysultanov D G, Salishchev G A et al. *Materials Letters*[J], 2015, 142: 153
- 23 Qiu Y, Hu Y J, Taylor A et al. *Acta Materialia*[J], 2017, 123: 115
- 24 Feng R, Zhang C, Gao M C et al. *Nature Communications*[J], 2021, 12(1): 4329
- 25 Huang X, Miao J, Luo A A. *Scripta Materialia*[J], 2022, 210: 114462
- 26 Yao H W, Liu Y M, Sun X H et al. *Intermetallics*[J], 2021, 133: 107187
- 27 Zhang Z J, Sheng H W, Wang Z J et al. *Nature Communications*[J], 2017, 8(1): 14390
- 28 Vaidya M, Muralikrishna G M, Murty B S. *Journal of Materials Research*[J], 2019, 34(5): 664
- 29 Zhi Q, Tan X R, Liu Z X et al. *Micron*[J], 2021, 144: 103 031
- 30 Sun W, Huang X, Luo A A. *Calphad*[J], 2017, 56: 19
- 31 Guo Yiqian, Guo Zhenghua, Li Zhiyong et al. *Rare Metal Materials and Engineering*[J], 2023, 52(8): 2965 (in Chinese)
- 32 Qi Yanfei, Ren Xiqiang, Zhou Jingyi et al. *Rare Metal Materials and Engineering*[J], 2022, 51(2): 735 (in Chinese)
- 33 Wang Z H, Chen S Y, Yang S L et al. *Journal of Materials Science & Technology*[J], 2023, 151: 41
- 34 Xu T, Chen Q J, Ji L et al. *Journal of Alloys and Compounds*[J], 2023, 956: 170179
- 35 Stepanov N D, Yurchenko N Y, Skibin D V et al. *Journal of*

- Alloys and Compounds*[J], 2015, 652: 266
- 36 Li M J, Chen Q J, Cui X et al. *Journal of Alloys and Compounds*[J], 2021, 857: 158278
- 37 Stepanov N D, Yurchenko N Y, Panina E S et al. *Materials Letters*[J], 2017, 188: 162
- 38 Lee K, Jung Y, Han J et al. *Materials*[J], 2021, 14(8): 2085
- 39 Xu Z Q, Ma Z L, Wang M et al. *Materials Science and Engineering A*[J], 2019, 755: 318
- 40 Liu X W, Bai Z C, Ding X F et al. *Materials Letters*[J], 2021, 287: 129255
- 41 Xu J L, Wang T, Lu Y F et al. *Materials Science and Technology*[J], 2020, 36(16): 1762
- 42 Huang X J, Miao J S, Luo A A. *Journal of Materials Science*[J], 2018, 54(3): 2271
- 43 Pei X H, Du Y, Hao X X et al. *Wear*[J], 2022, 488: 204166
- 44 Yurchenko N Y, Stepanov N D, Zherebtsov S V et al. *Materials Science and Engineering A*[J], 2017, 704: 82
- 45 Stepanov N D, Yurchenko N Y, Shaysultanov D G et al. *Materials Science and Technology*[J], 2015, 31(10): 1184
- 46 Liu K, Li X, Wang J Y et al. *Materials Characterization*[J], 2023, 200: 112878
- 47 Yurchenko N, Panina E, Tikhonovsky M et al. *Materials Letters*[J], 2020, 264: 127372
- 48 Jiang W T, Wang X H, Kang H J et al. *Journal of Alloys and Compounds*[J], 2022, 925: 166767
- 49 Wang M L, Lu Y P, Lan J G et al. *Acta Materialia*[J], 2023, 248: 118806
- 50 Senkov O N, Rao S, Chaput K J et al. *Acta Materialia*[J], 2018, 151: 201
- 51 Chauhan P, Yebaji S, Nadakuduru V N et al. *Journal of Alloys and Compounds*[J], 2020, 820: 153367
- 52 Liu K, Wang J Y, Li X et al. *Materials Science and Engineering A*[J], 2023, 869: 144779
- 53 Stepanov N D, Yurchenko N Y, Sokolovsky V S et al. *Materials Letters*[J], 2015, 161: 136
- 54 Gao F, Sun Y, Hu L X et al. *Journal of Alloys and Compounds*[J], 2023, 932: 167659
- 55 Yurchenko N Y, Stepanov N D, Shaysultanov D G et al. *Materials Characterization*[J], 2016, 121: 125
- 56 Tan X R, Zhao R F, Ren B et al. *Materials Science and Technology*[J], 2016, 32(15): 1582

Al-Ti-V 基轻质高熵合金研究现状

薛源, 单贵斌, 潘瑞林, 唐颂, 兰司

(南京理工大学 材料科学与工程学院, 江苏 南京 210094)

摘要: 近年来, 高熵合金凭借其新颖的设计理念和优异的各类物化性能成为金属结构材料领域的研究热点。随着轻量化合金设计理念的不断普及, “熵调控”的概念也被广泛应用于开发新型轻质合金。轻质高熵合金是基于合金轻量化设计的一类低密度的新型高熵合金, 其开发与设计主要利用经验参数准则、相图计算以及第一性原理计算相结合的方法。其中, Al-Ti-V 基轻质高熵合金凭借其优异的力学性能、良好的高温抗氧化性及耐腐蚀性等优点, 受到了广泛关注。本文基于 Al-Ti-V 基轻质高熵合金的研究现状, 从成分设计、制备方法、结构特征以及各类物化性能特点等方面进行了综述, 并指出了 Al-Ti-V 基轻质高熵合金所面临的问题与挑战。

关键词: 轻质高熵合金; 合金设计; 制备方法; 微观组织; 物化性能

作者简介: 薛源, 男, 2000年生, 硕士, 南京理工大学材料科学与工程学院, 江苏 南京 210094, E-mail: 121116223511@njust.edu.cn